Title
PRECIPITATION OF TiC IN THERMALLY EMBRITTLED MARAGING STEELS

Author
Nes, E.

Publication Date
1976-02-01

Submitted to Metallurgical Transactions

LBL-3927
Preprint c.1

PRECIPITATION OF TiC IN THERMALLY EMBRITTLED MARAGING STEELS

E. Nes and G. Thomas

February 1976

Prepared for the U. S. Energy Research and Development Administration under Contract W-7405-ENG-48

LBL-3927

PRECIPITATION OF TiC IN THERMALLY EMBRITTLED MARAGING STEELS

E. Nes* and G. Thomas

Department of Materials Science and Engineering, College of Engineering, and Inorganic Materials Research Division, Lawrence Berkeley Laboratory, University of California, Berkeley, California 94720

ABSTRACT

It is shown that maraging steels can be embrittled by the precipitation of TiC during slow cooling and/or intermediate annealing in the austenite temperature range. An important aspect in this embrittlement is the occurrence of lamellar precipitation of TiC at the austenite grain boundaries, generating a cellular structure of large fern leaf-like carbides. Within the austenite grains a non-uniform distribution of irregularly plate - shaped TiC particles are formed with {100} austenite habit orientation. Quenching to martensite, prior to any intermediate anneals, change the carbide distribution upon subsequent annealing treatments into a fine dispersion of TiC particles. The embrittlement resulting from the various isothermal annealing treatments in the austenite temperature region could all be directly related to the carbide distribution in the prior austenite grain boundary region.

* Present address: Central Institute for Industrial Research, Blindern, Oslo 3, Norway.

INTRODUCTION

Maraging steels belong to a class of low carbon high alloyed steels which attain their strength by precipitation-hardening[1,2]. The typical heat treatment of these alloys consists of a solution treatment at about 800-900°C followed by air cooling to room temperature to form a highly dislocated lath-like iron-nickel martensite. Upon aging at 450 to 500°C a fine dispersion of Ni_3Mo and Ni_3Ti forms along dislocations and lath boundaries left by the martensitic transformation[3-5]. The tensile strength attained is in the range 200-300 ksi and if the alloy is properly heat treated, this high strength level is combined with excellent fracture toughness properties. However, severe toughness degredation, characterized by a complete intergranular fracture mode, may result if the material is improperly heat treated. For example if it is subjected to a too high solution annealing temperature followed by slow cooling, or an intermediate annealing treatment in the austenite temperature region. This phenomenon, termed "thermal embrittlement" has in recent years been the subject of several investigations[6-9], and the various proposed models for the embrittling mechanism are all concerned with grain boundary segregation and/or precipitation of alloy carbides or nitrides. Precipitation reactions at prior austenite grain boundaries in 18%Ni-Co-Mo steel after heating at 1200°C and then maintained at 750°C was first reported by Hall and Campbell[10]. The later work of Boniszewski and Boniszewski[11] attributed the formation of such grain boundary particle networks to the precipitation of TiC or possibly a titanium carbonitride. Boniszewski and Boniszewski also suggested that these networks may be detrimental to the impact properties of marging steels.

Only recently has this thermal embrittlement been the subject of more systematic investigations[8,9]. Kalish and Rack[8] established the temperature range of the thermal embrittlement and attributed the major loss in toughness to the diffusion of interstitial impurity atoms as carbon and nitrogen to the austenite grain boundaries during cooling or intermediate isothermal annealing below 1100°C. The discrete precipitation of Ti (CN) at the boundaries was believed to play a role only in the advanced stage of the embrittlement. Johnson and Stein[9] examined the cause of thermal embrittlement by employing Auger electron spectroscopy and showed that the embrittlement was directly correlated with segregation of Ti and C to the prior austenite grain boundaries. They proposed that embrittlement was then due to subsequent reaction of Ti and carbon to form a carbide at the boundaries.

Although it appears that thermal embrittlement requires the presence of Ti and C(N) in the prior austenite grain region, the separate effects of atomic grain boundary segregation and boundary inclusions cannot be considered resolved by the above works as no direct observations were made of the particle structure resulting from the embrittling heat treatments. Accordingly, in order to understand better the detailed mechanism by which the grain boundaries are embrittled during slow cooling or intermediate isothermal annealing in the austenite temperature range, an objective of this work is to characterize the precipitation products in the prior austenite grain boundary regions as well as within the grains. From the characterisation results, the precipitation behaviour may be changed by altering the heat treatment schedule so as to determine whether changing the carbide distribution affectsthe fracture properties. The results were compared to those obtained by conventional heat treatments.

EXPERIMENTAL

The experimental data obtained in this work pertains to a commercial 250 grade maraging steel of the composition given in Table I. This material was provided in the wrought condition as cylindrical rod stock, 1/2 inch diameter.

Specimens from two heat treatment series have been investigated. One series (heat treatment I) was heat treated so as to ensure a maximum embrittlement effect[8,9] viz., a high temperature solution treatment at about 1300°C for 1 hour followed by a direct quench to 870°C with subsequent anneals at 870°C for various times. For heat treatment II the material was quenched to martensite following the 1300°C solution anneal and then reheated and aged at 870°C. The α-γ transition during heating of maraging steels has been reported to be a reversible shearing process[12,13] producing a highly dislocated austenite, which if heated to some suitable temperature above the transformation temperature may recrystallize to a fine austenite grain size[14]. In the present case the objectives of the quench to martensite from the solution treatment was to examine if these aspects of the martensitic α-γ transformation in the maraging steels will alter the carbide distribution during the subsequent intermediate 870°C annealing treatment. During all heat treatments the specimens were contained in evacuated quartz capsules.

The size, distribution and chemical nature of the decompostion products resulting from these heat treatments have been established by combining optical metallography, transmission electron microscopy and electron microprobe investigation. Surface metallography was especially helpful in determining certain aspects of the decomposition reactions involved as it was discovered that by mechanical overpolishing,the morphology of the larger grain boundary particles could be revealed in surprisingly great details as shown in Figs. 1 and 2a. This preparation technique is far superior to the various recommended Nital etching procedures[11] for revealing inclusions and prior austenite grain boundaries.

Simple tensile tests were conducted in order to examine the effects of the various heat treatments on the mechanical properties. The specimens were subjected to a one hour intermediate embrittling anneal and their properties compared to specimens given a conventional solution treatment (4 hours at 820°C and air cooled). All specimens were subsequently aged to peak hardness, i.e. 3 hrs at 480°C before tensile testing. The detailed nature of the various fracture surfaces was examined by SEM.

RESULTS AND DISCUSSION

In order to distinguish the precipitates due to the embrittling intermediate anneal from the particle structure present at the termination of the high temperature treatment, foils for TEM work were prepared from material subjected to the high temperature treatment only. In the as-quenched condition this highly dislocated lath-like martensite contained a low density of relatively large (>1μm diameter) particles assumed to be remnants from the alloy casting. While these inclusions were not subjected to any detailed diffraction pattern analysis, d-values associated with the majority of the inclusions examined could be ascribed to Ti(CN). A few inclusions believed to be TiS_2 were also detected[11].

Particle Distribution, Morphology and Structure (Heat Treatment I)

The particle structure emanating from the intermediate annealing treatment is characterized by two types of precipitates determined by the site of their formation, viz., formed within the prior austenite grains or in the grain boundary region. Important aspects of the grain boundary precipitation reactions could be conveniently studied by the surface metallographic technique described above, as illustrated by the optical micrographs in Fig. 1. On the scale of these micrographs considerable local variation in the extent of the austenite grain boundary precipitation is observed. Some boundaries appear as strings of particles revealing a simple boundary decoration by TiC, while other boundaries are associated with far more complicated particle configurations. As detailed by the optical and TEM micrographs in Fig. 2a and b, the grain boundary precipitation reaction may result in a network of long fern leaf-like particles and more irregular dendritic shaped inclusions. The size and morphology of these particles resemble those observed by Boniszewski and Boniszewski[11] studying carbon replicas from grain boundary embrittled fracture surfaces of a maraging steel.

Within the prior austenite grains irregular plate shaped particles illustrated by the TEM micrograph in Fig. 3, were observed. These precipitates were exceedingly non uniformly distributed with large volume fractions almost particle free, while other regions contained clusters of high particle density as shown in Fig. 3a. On a more macroscopic level the optical micrograph in Fig. 1c shows a high precipitate particle density within the diffusional zones surrounding the cast-in inclusions. The plate shaped particles observed in the TEM micrographs reached after about 3 hours annealing time a diameter of 0.2-0.3μm with the thickness in the 200-400Å range. A typical feature is their frequent distribution into rows as shown in Fig. 3a. This non-uniform distribution pattern into clusters and rows of particles is assumed to reflect the heterogeneous nature by which these particles are nucleated, mapping out the low density of subgrain boundaries and dislocation tangles still present within the prior austenite grains after the high temperature solution anneal.

A series of transmission electron diffraction patterns from individual precipitate particles tilted into different lattice orientations have been analysed and both the grain boundary region particles as well as the plate shaped particles were found to have a face centered cubic structure with lattice parameter 4.32±0.05Å. The precipitate diffraction pattern in Fig. 4 shows a particle situated in the bcc martensitic matrix of [111] orientation so that [111] martensite parallels [110] precipitate. Both TiC and TiN have f.c.c. lattices with parameters 4.33Å and 4.21 Å respectively (11). However, the uncertainty in the present experimentally determined lattice parameter is less than the 2% difference between these two lattices, and accordingly it is concluded that in the present case the decomposition product is TiC.

The orientation relationship between the f.c.c. TiC particles and the martensite shown in Fig. 4 has been observed both for the plate shaped particles and the larger grain boundary inclusions. As can be seen from Fig. 4 the (110) plane of the particle is close to the (111) of the martensite, with the $[\bar{1}1\bar{1}]$ particle vector at an angle of approximately 24° with respect to the $[\bar{1}10]$ vector of the martensite. By observing the Kurdjumov-Sachs austenite-martensite orientation relationship this is consistent with TiC particles precipitating in twin orientation with the f.c.c. austenite.

The habit plane of these particles was determined by tilting experiments as exemplified in Fig. 4. By rotating Fig. 4a into a [110] orientation, Fig. 4b, the particles A,B,C and D are all seen edge-on while the particles E anf F are nearly in an edge-On orientation and at angles approximately 90° and 45° respectively to the A-D particles. By again observing the K-S austenite-martensite orientation relationship this tilting result is consistent with the plate shaped TiC precipitates having {100} austenite lattice habit orientations.

The Grain Boundary Precipitates

The optical micrographs in Fig. 1 illustrate that the TiC precipitates are heterogenously nucleated on the austenite grain boundaries during the intermediate annealing treatment. The detailed micrographs of Fig. 1b and d suggest a dynamic role played by the grain boundary in this decomposition process, indicating that grain boundary migration is involved, i.e. a discontinuous precipitation reaction. However, as hetergeneous nucleation and plate like growth of lamellae precipitates can occur at grain boundaries without requiring discontinuous precipitation, the details of the kinetics of the present grain boundary reaction had not been resolved.

The scale of the present grain boundary precipitates is at variance with the results reported by Johnson and Stein[9] who interpreted their Auger electron spectroscopy data as indicating a strong segregation of Ti into a narrow grain boundary zone of approximately 400Å thickness. It is difficult to conceive a thermodynamical force responsible for such a distributuion and it is suggested that topography effects may be responsible for their results. It is interesting to observe that the thickness of the segregated boundary regions reported by Johnson and Stein is of the same scale as the thickness of the leaf-like grain boundary region particles. The fracture analysis given below shows that these particles form the only microscopically flat sections of the fracture surface which are not truly intergranular on a high magnification scale. These observations may provide an alternative interpretation to the Johnson and Stien "segregation" as the flat regions of exposed TiC on the fracture surface may dominate in the Auger spectrum of embrittled maraging steels. When these particle remnants have been sputtered away the bulk Ti-concentration is obtained.

Effect of Quenching From Solution Treatment (Heat Treatment II)

As anticipated, quenching to martensite prior to the intermediate 870°C anneal had a major effect on the decomposition behaviour of the supersaturated Fe-Ti-C solid solution. While after heat treatment I the particle distribution was exceedingly non-uniform, the result of this treatment was a nearly uniform distribution of finely dispersed particles. As can be seen from the transmission electron micrograph in Fig. 5a, these particles no longer have the plate shaped morphology characteristic of heat treatment I, but are of a globular shape. Although some evidence of grain boundary precipitation was observed, Fig. 5b, no lamellar precipitation could be detected. Diffraction pattern analysis of these particles gave the same structural result as reported above, i.e. they are TiC. This change in precipitation behaviour as compared to the other heat treatment is attributed to the initial presence of a high dislocation density in the material (resulting from the $\alpha \rightarrow \gamma$ transformation (12,13)) during the intermediate anneal, providing nucleation sites for the carbides. During heat treatment I the direct quench to 870° gave a material which was assumed to be virtually distortion free within the γ-grains. No significant grain boundary refinement effect was observed to result from the temperature cycling to room temperature and back to the intermediate annealing temperature. This is in accordance with the results reported by Hall et al (13) who concluded that grain refinement in maraging steels cannot be accomplished without strain to cause recrystallization of the austenite. However, the later work by Saul et al (14) demonstrated that substantial grain refinement may be achieved by thermal cycling alone, provided that the thermal cycle is from a temperature below M_f to a temperature considerably above the austenitizing temperature. Why no grain refinement was obtained in the present case may be due to either a too low intermediate annealing temperature or the possibility that the finely dispersed TiC particles nucleate and grow at a rate sufficient to inhibit the recrystallization reaction.

Mechanical Properties

The results of the tensile tests are given in Table II and as can be seen the excellent ductile properties of the conventionally heat treated material are severely impared by the embrittling heat treatments.

Heat treatment I caused a complete embrittling of the material with some specimens even failing prior to general yielding. The effect of heat treatment II is less dramatic but still causes substantial ductility degradations.

Details of the various fracture modes are given in Figs. 6 to 8. The conventionally heat treated material failed by a cup and cone type fracture involving a substantial reduction in area. A characteristic fracture surface feature of this material was the "giant" dimples, Fig. 6a, apparently nucleated by quasi cleavage or fracturing of large inclusions assumed to be Ti-rich phases, Fig. 6b. The relatively high density of these dimples on the fracture surfaces suggests that these large inclusions play a major role in limiting the overall plasticity of the material. This observation is in agreement with a recent work by Cox and Low[15] showing that in 200 grade maraging steels the plastic fracture takes place through void initiation by the titanium carbo-nitride inclusion.

The heat treatment I fracture surfaces appear on a low magnification scale as completely intergranular, Fig. 7a. The more detailed fractographs of Fig. 7b and c exhibit a more complicated surface topography revealing that some plastic tearing is involved. The salient fracture aspect of this material is the straight ridge pattern, apparently mapping out a set of crystallographic directions , Fig. 7b. The fracture Charpy specimens investigated by Kalish and Rach[8] and Johnson and Stein[9] displayed similar features, and from the geometry of intersecting ridges (or by stereo analysis) these ridges can be seen to form flat steeply inclined surfaces, while the regions in between appear as a result of ductile rupture, Fig. 7c. The occurrence of such a fracture surface can now be conveniently explained in terms of the precipitation mode suggested schematically in Fig. 9a. In terms of this model the effect of the grain boundary is to provide a macroscopic continuous fracture path, while on the microscopic level the fracture is a mixed mode type consisting of a quasicleavage and dimple rupture.

The heat treatment II material was less brittle and the fracture of a mixed mode (both trans- and intergranualr) type, Fig. 8a. Details from an intergranularly fractured region are given in Fig. 8b showing a uniform distribution of small dimples. This change in intergranular fracture surface topography as compared to the heat treatment I material is consistent with the change in carbide distribution in the prior austenite grain region from large discontinuously formed particles resulting from heat treatment I to the much smaller grain boundary particles in heat treatment II, Fig. 5b. Another aspect of the fracture behaviour of this heat treatment is that the transgranularly fractured regions, as shown in Fig. 8c, do not display a heavily dimpled structure like the conventionally heat treated material, but exhibit much smaller dimples which follow almost smoothly curved surfaces. This transgranular fracture pattern is interpreted as a <u>subgrain boundary</u> fracture mode. Fig. 9b schematically outlines how the fracture path in heat treatment I material can follow either the high angle boundaries or the subgrain boundaries which both are decorated by finely dispersed TiC particles.

To summarize, the salient experimental results are that the fracture properties of thermally embrittled maraging steels are closely related to the presence of carbides in the prior austenite grain boundary regions.

The formation of carbides at these boundaries (as well as within the prior austenite grains) during the various embrittlement heat treatments can be fully accounted for in terms of a nucleation and growth phenomenon occurring in a supersaturated iron-titanium-carbon solid soution. The possibility of having substantial segregation of Ti and/or C to the grain boundary region as suggested by some investigators (8,9) is less concievable in terms of such a decomposition mechanism, since the latter implies that throughout the entire embrittlement intermediate anneal both the Ti and C concentrations in the austenite grains as well as in the carbide-martensite interface will remain approximately constant, i.e. at the level of thermal equilibrium. Although the details of the ternary Fe-Ti-C equilibrium phase diagram in the temperature regions of this investigation have not been established, both the scale and the rate of this decomposition reaction implies that these equilibrium levels are substantially lower than the average bulk concentrations of Ti and C. Accordingly, rather than being a segregation effect, the decline in fracture toughness with increasing intermediate annealing times as observed by Kalish and Rack (8) and Johnson and Stein (9) is interpreted as being due to the observed increase in the volume fraction of grain boundary precipitates.

However, other impurity segregation effects may play an important role in the thermal embrittlement process, as trace ammounts of a series of elements such as Sb, Sn, As, P, Te, Bi, Se or Ge have been shown to induce grain boundary embrittlement in alloy steels. The various mechanisms by which such embrittlement may occur has recently been elegantly explored by Rellick and McMahon (16) and both their "carbide growth/impurity partition" model and the equilibrium segregation mechanism may be relevant in the analysing of the cohesive strength of the TiC-martensite interface. Future work should therefore concentrate on investigating thermal embrittlement in vacuum melted high purity maraging steels as well as materials with controlled impurity additions.

SUMMARY

1. A too high solution treatment of maraging steels may leave Ti and C in solid solution in sufficient amounts to cause the precipitation of TiC during subsequent slow cooling and/or intermediate annealing treatments in the austenite temperature range.

2. During such heat treatments lamellaer precipitation from the austenite grain boundaries causes the generation of a cellular structure of large fern leaf like carbides. Within the austenite grains a non-uniform distribution of irregularly plate shaped TiC particles are formed. These plate shaped particles grow with a {100} austenite habit orientation. The non-uniform distribution suggests a heterogeneous carbide nucleation, and the growth rates observed are consistent with a diffusion controlled decomposition process.

3. Quenching to martensite prior to any intermediate anneals in the austenite range changes the decomposition pattern upon subsequent annealing treatments. No precipitation occurred at the austenite grain boundaries, and within the grains a uniform distribution of finely dispersed TiC particles was observed.

4. The embrittlement resulting from the present heat treatments could all be directly related to the carbide distribution in the prior austenite grain boundary region.

5. An important aspect of future research is to explore the possible effects of impurity segregation on the decohesion stress of the TiC-martensite interface. Such an analysis has implications also on non-embrittled material as such decohesion from cast-in TiC particles may limit the overall plasticity of the maraging steels.

ACKNOWLEDGEMENTS

The authors wish to express their gratitute to the U.S. Energy Research and Development Administration for financial support. We are also thankful to the Precision Founders Inc. for supplying the alloy. One of us (E.N.) wants to thank the Royal Norwegian Council for Industrial and Scientific Research for financial support.

1. R. F. Deker, J. T. Each, and A. J. Goldman, Trans. ASM, 1962, Vol 55, p. 58.
2. S. Floreen, Met. Rev., Review 126, 1968, p. 115.
3. A. J. Baker and P. R. Swann, Trans. ASM, 1964, Vol 57, p. 1009.
4. G. P. Miller and W. I. Mitchell, J. Iron Steel Inst. 1965, Vol 203, p. 899.
5. J. Lin Cheng and G. Thomas, Trans. ASM, 1969, Vol 62, p. 852.
6. C. J. Barton, B. G. Reisdorf, P.H. Salmon Cox, J. M. Chilton and C. E. Oskin, AFML-TR-67-34, (1967).
7. G. F. Spaeder, Met. Trans., 1970, Vol 1, 2011.
8. D. Kalish and H. F. Rack, Met. Trans, 1971, Vol. 2, 2665.
9. W. C. Johnson and D. Stein, Met. Trans., 1974, Vol 5, 549.
10. A. M. Hall and J. E. Campbell, "Report on the Fourth Maraging Steel Project Review," DMIC 1964. Battelle Memorial Institute.
11. T. Boniszewski and E. Boniszewski, J. Iron & Steel Inst. 1964, Vol. 204, 340.
12. A. M. Hall, Metall. Handbook, Vol 2, 8th ed. p. 255, Am. Soc. Metals, Novelty, Ohio, 1964.
13. A. M. Hall, R. C. Simon and D. P. Moon, DMIC Processes and Properties Handbook, 1968, Battelle Memorial Institute, Columbus, Ohio.
14. G. Saul, J. A. Roberson, and A. M Adair, Met. Trans., 1970, Vol. 1, p. 383.
15. T. B. Cox and J. R. Low, Met. Trans., 1974, Vol 5, p. 1457.
16. J. R. Rellick and C. J. McMahon, Met. Trans., 1974, Vol 5, p. 2439.

TABLE I

Chemical Analysis of the Alloy

Element	Composition (Wt %)
Ni	18.7
Co	7.7
Mo	4.9
Ti	0.43
C	0.01
N	not determined

TABLE II

Tensile Mechanical Property Results

Material	0.2 Yield Stress		True Fracture Stress		Elong. %	R.A. %
	ksi	MN/m^2	ksi	MN/m^2		
Conventional Heat Treatment	257	1.77×10^3	410	2.83×10^3	11.5	65
Heat Treatment I	234	1.61×10^3	236	1.63×10^3	~0	~0
Heat Treatment II	258	1.78×10^3	275	1.90×10^3	1.8	9.5

FIGURE CAPTIONS

Fig. 1. a) Optical micrograph showing the decorated prior austenite boundaries as revealed by mechanically overpolishing (heat treatment I material). b) and c) are optical micrographs and d) a SEM micrograph of the regions marked out in a).

Fig. 2. a) Typical distribution of particles in the prior austenite region (optical micrograph), and b) TEM micrograph of a fern leaf-like grain boundary region particle.

Fig. 3. a) TEM micrograph of plate shaped particles resulting from a 3 hr at 870°C annealing treatment. b) The same foil in a (100) lattice orientation showing the particles A-F nearly edge on and oriented at 90° and 45° with respect to each other.

Fig. 4. Matrix (m) and precipitate (p) diffraction patterns showing the martensite in a nearly (111) orientation while the face centered cubic lattice of the particle (TiC) is in a (110) orientation.

Fig. 5. a) Typical carbide distribution resulting from heat treatment II material, viz., solution treatment followed by quenching to martensite and an intermediate anneal at 870°C. b) TiC decorated prior austenite subgrain boundary.

Fig. 6. Ductile fracture surface of conventionally heat treated maraging steel, a) the large dimples (arrows) are initiated by quasi-cleavage from particles, b) assumed to be cast in Ti-rich phases.

Fig. 7. Prior austenite grain boundary fracture resulting from heat treatment I. The straight ridges, b) and c), form flat, slightly inclined, regions due to quasi cleavage from the discontinuously formed TiC particles.

Fig. 8. a) Mixed mode fracture of heat treatment II material. b) Finely dimpled intergranual fracture surface. c) The transgranular fracture path is assumed to follow the TiC decorated prior austenite subgrain boundaries.

Fig. 9. Schematic representation of the embrittlements due to, a) the discontinuously formed carbides of heat treatment I, and b) the finer dispersion of TiC decorating the high and low angle prior austenite boundaries of heat treatment II.

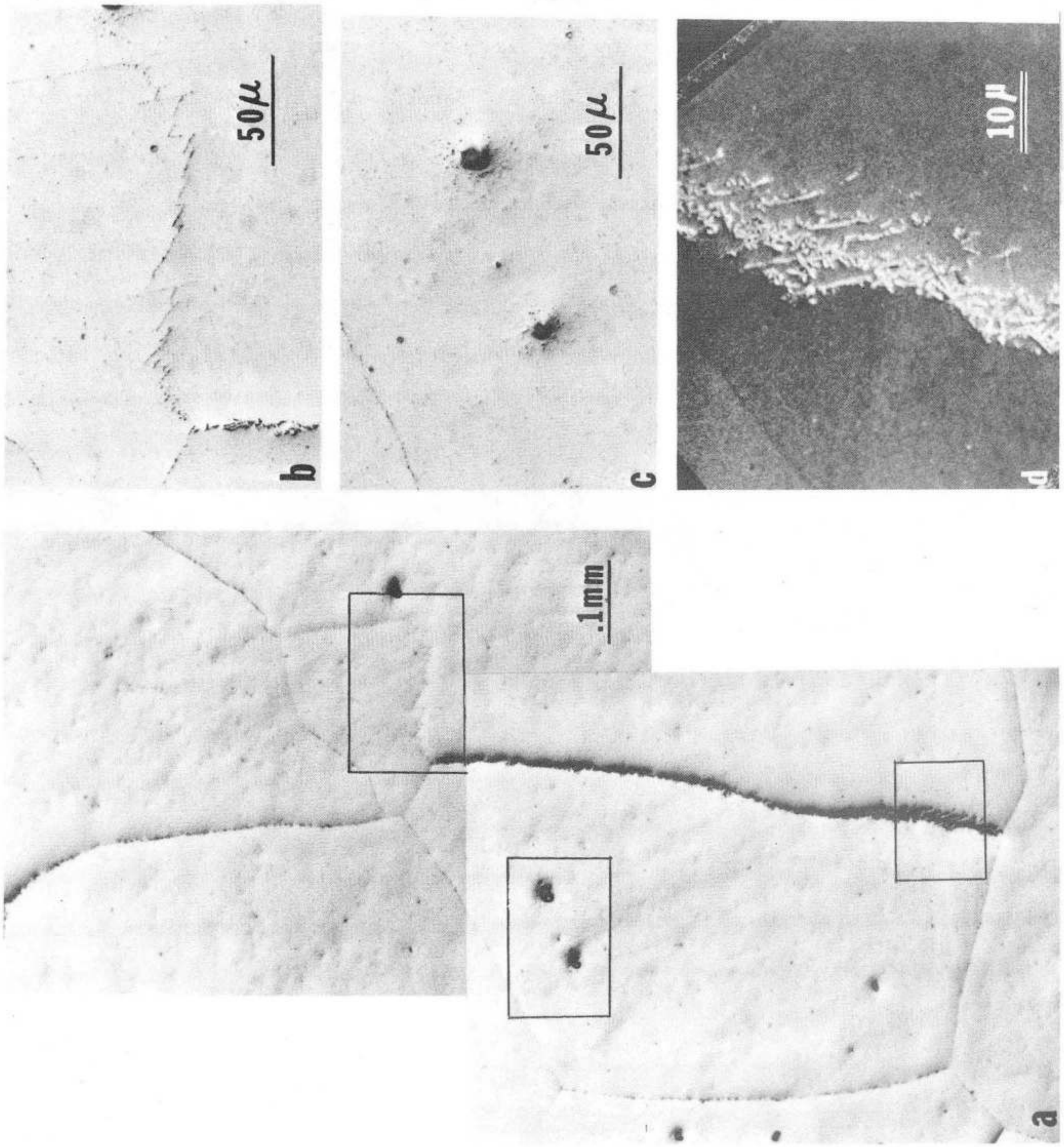

Fig. 1

XBB 755-3894

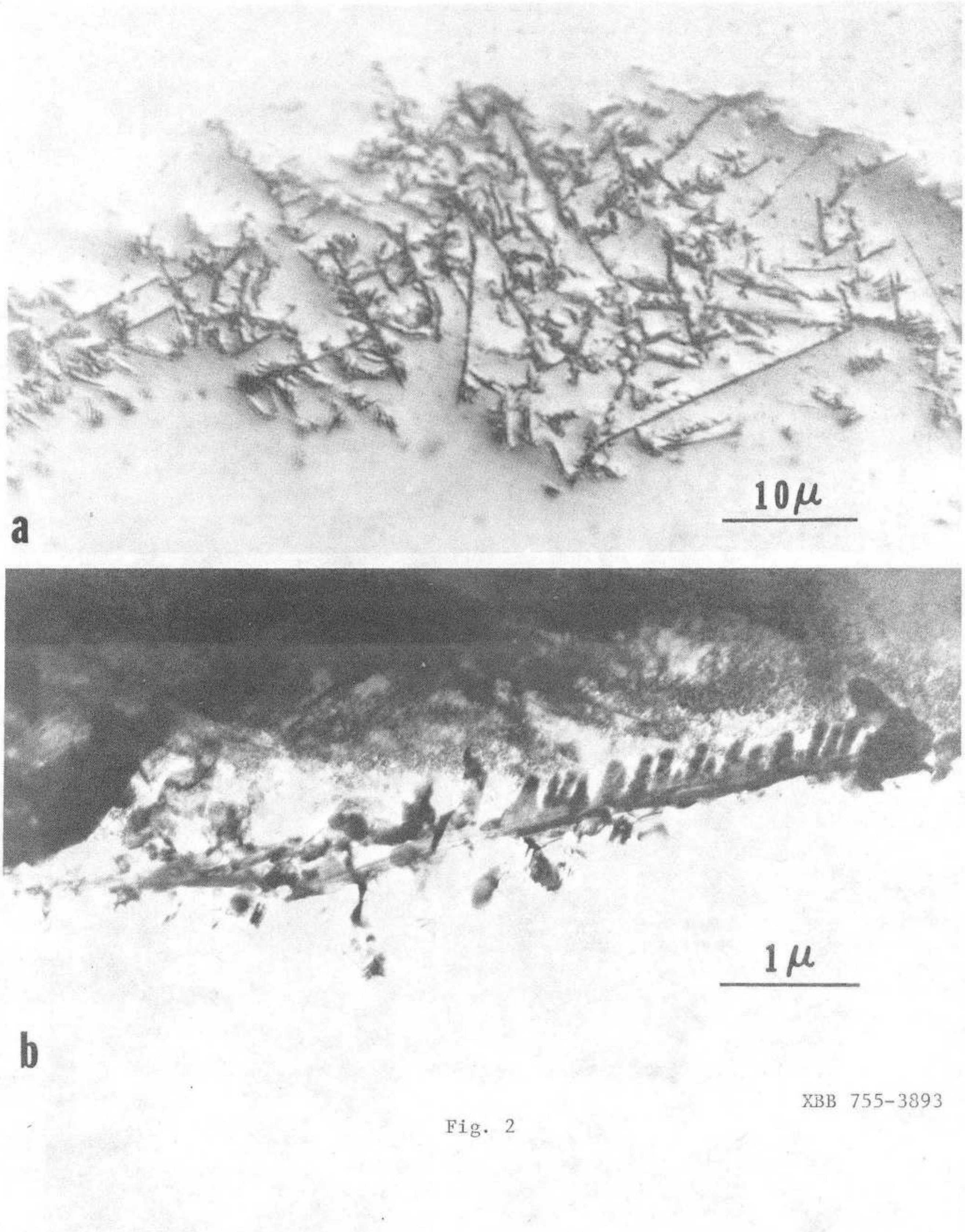

XBB 755-3893

Fig. 2

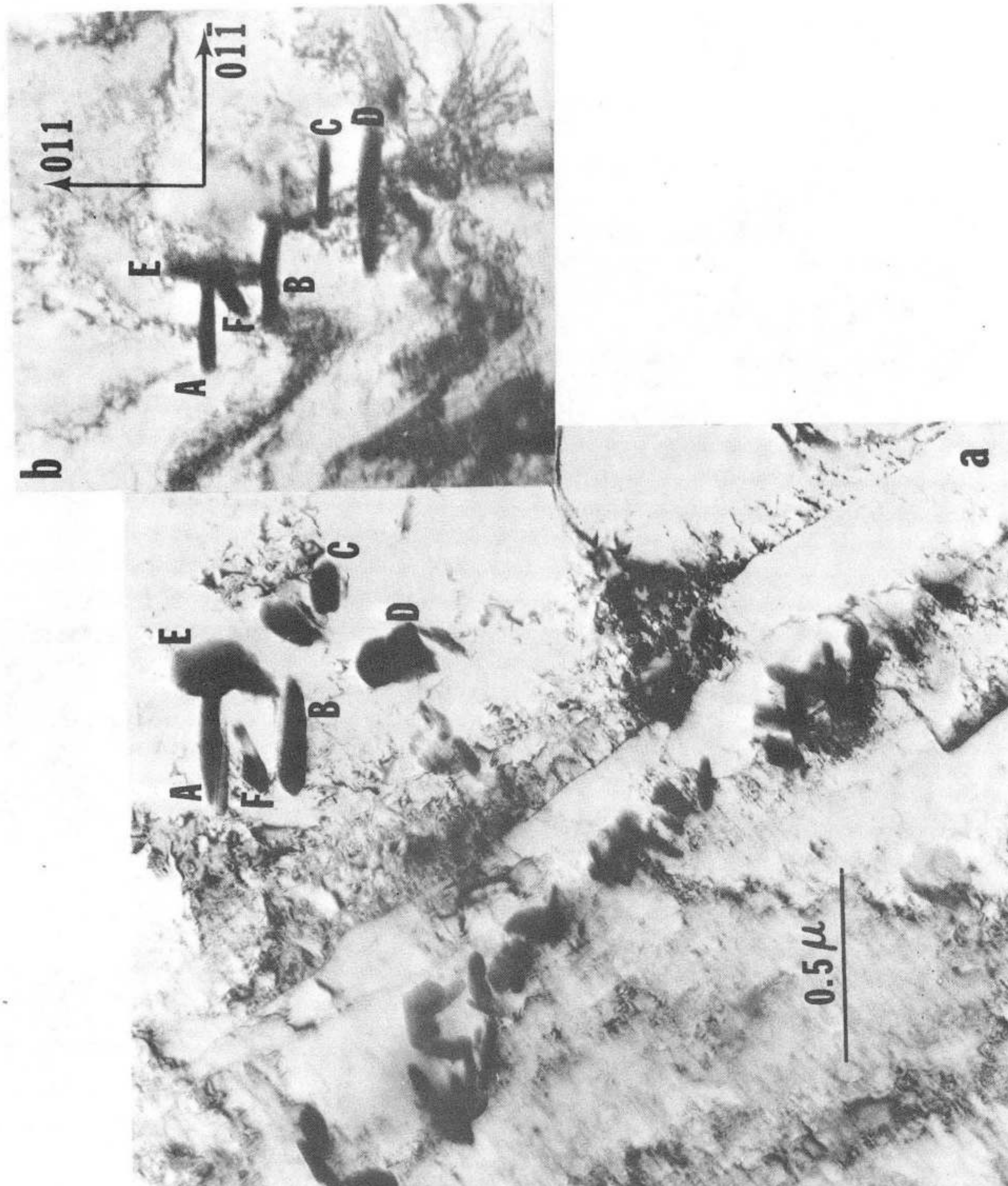

Fig. 3

XBB 755-3895

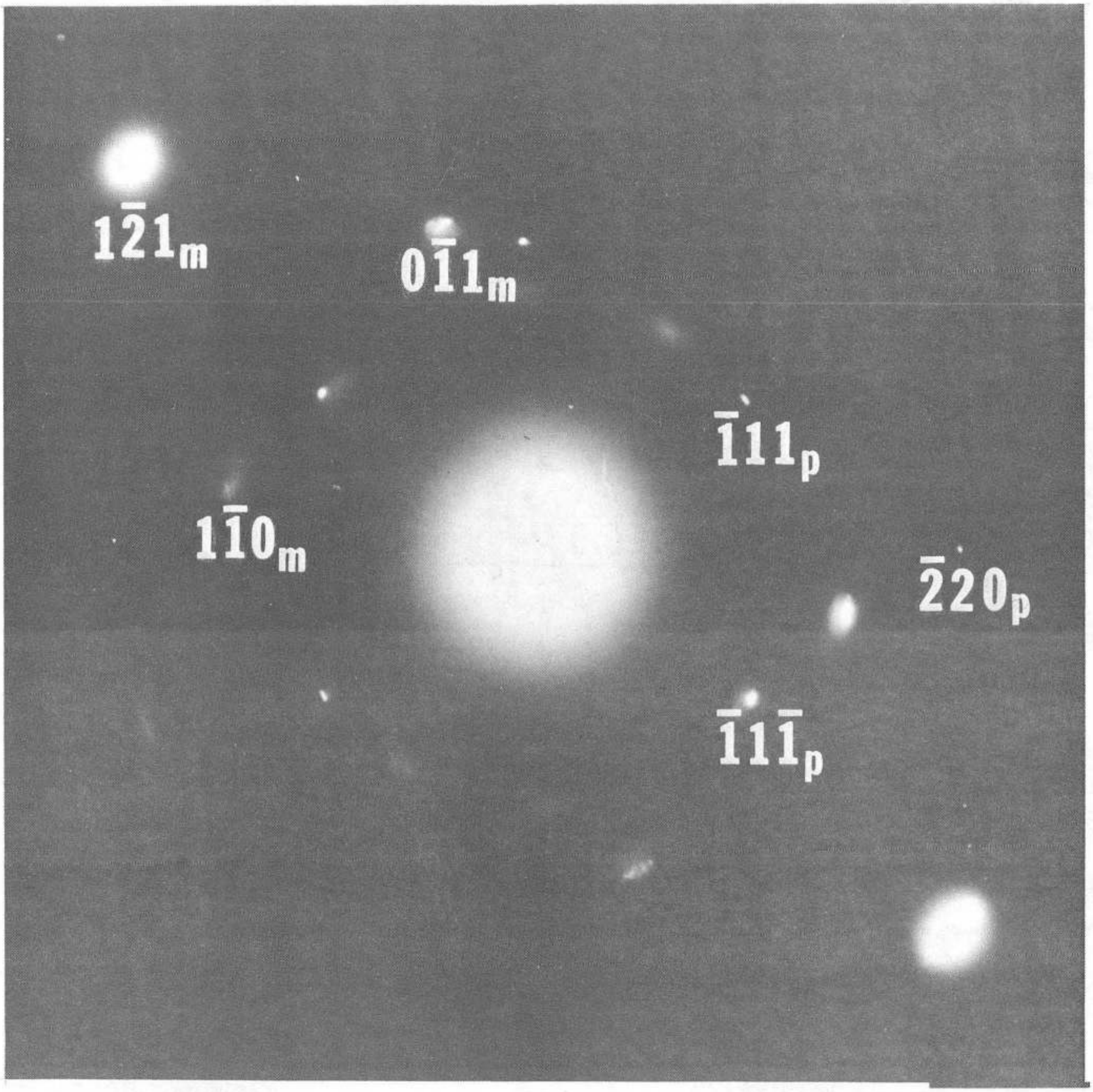

XBB 755-3892

Fig. 4

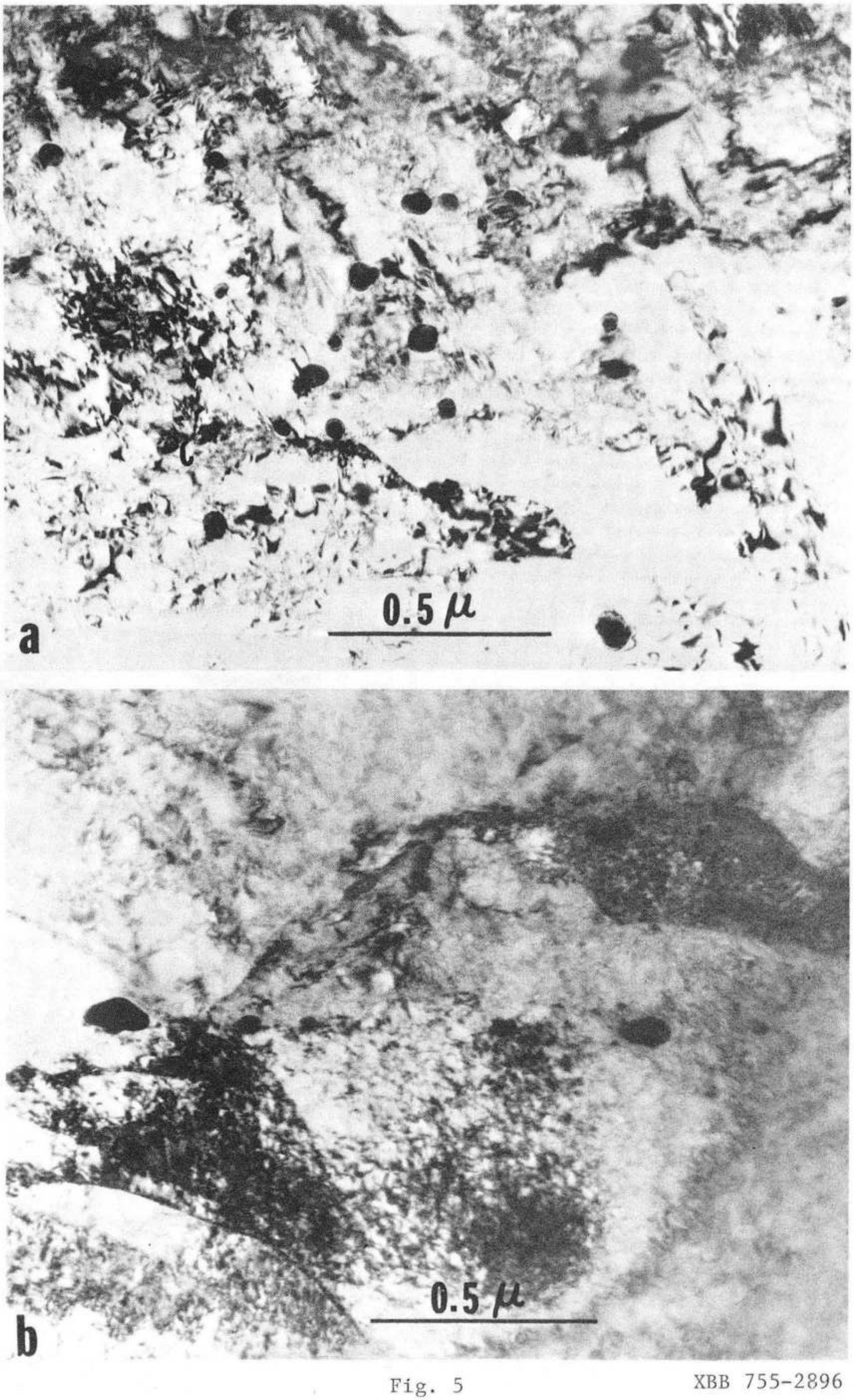

Fig. 5 XBB 755-2896

0 0 0 0 4 3 0 5 5 5 4

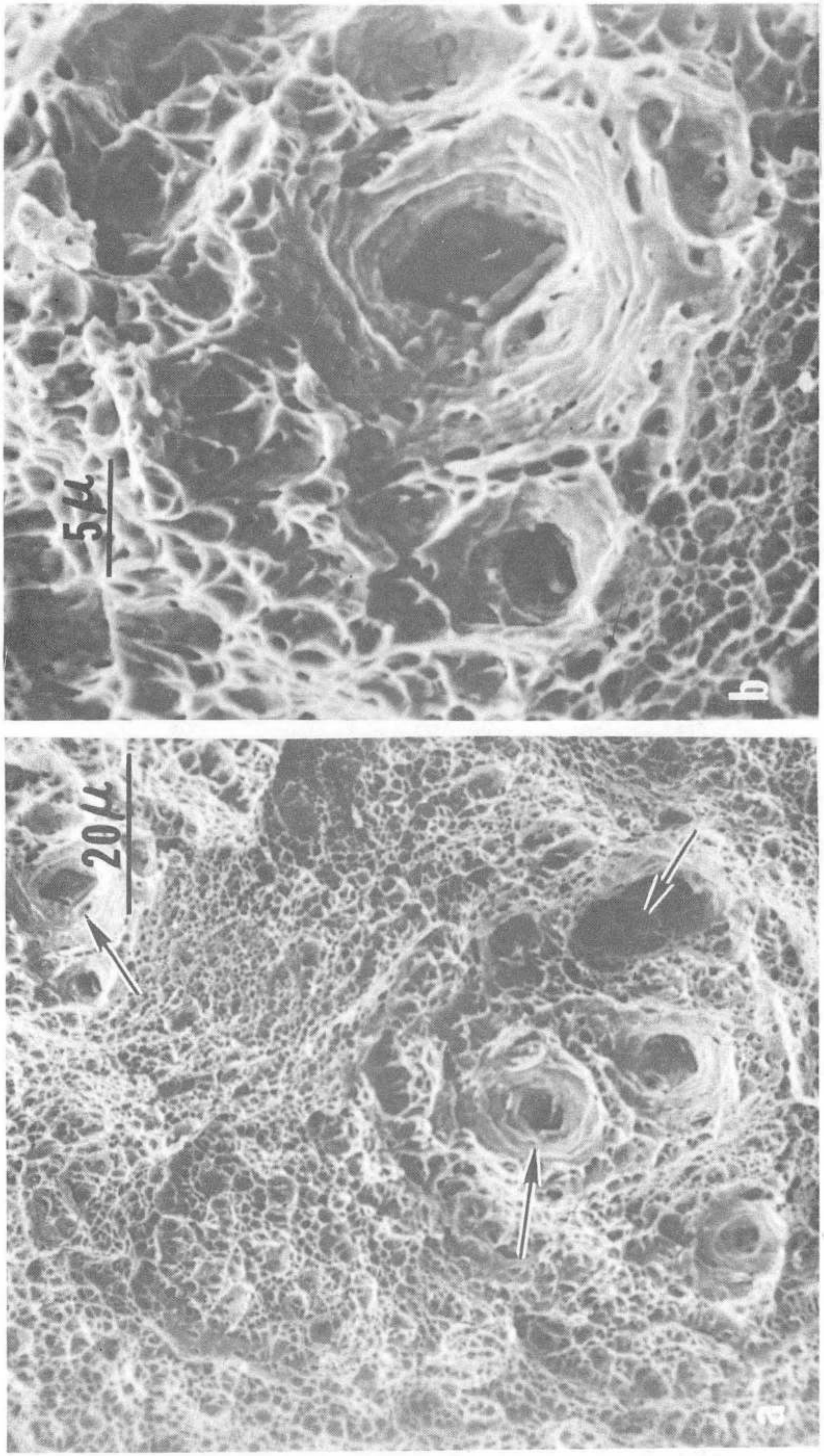

XBB 755-3897

Fig. 6

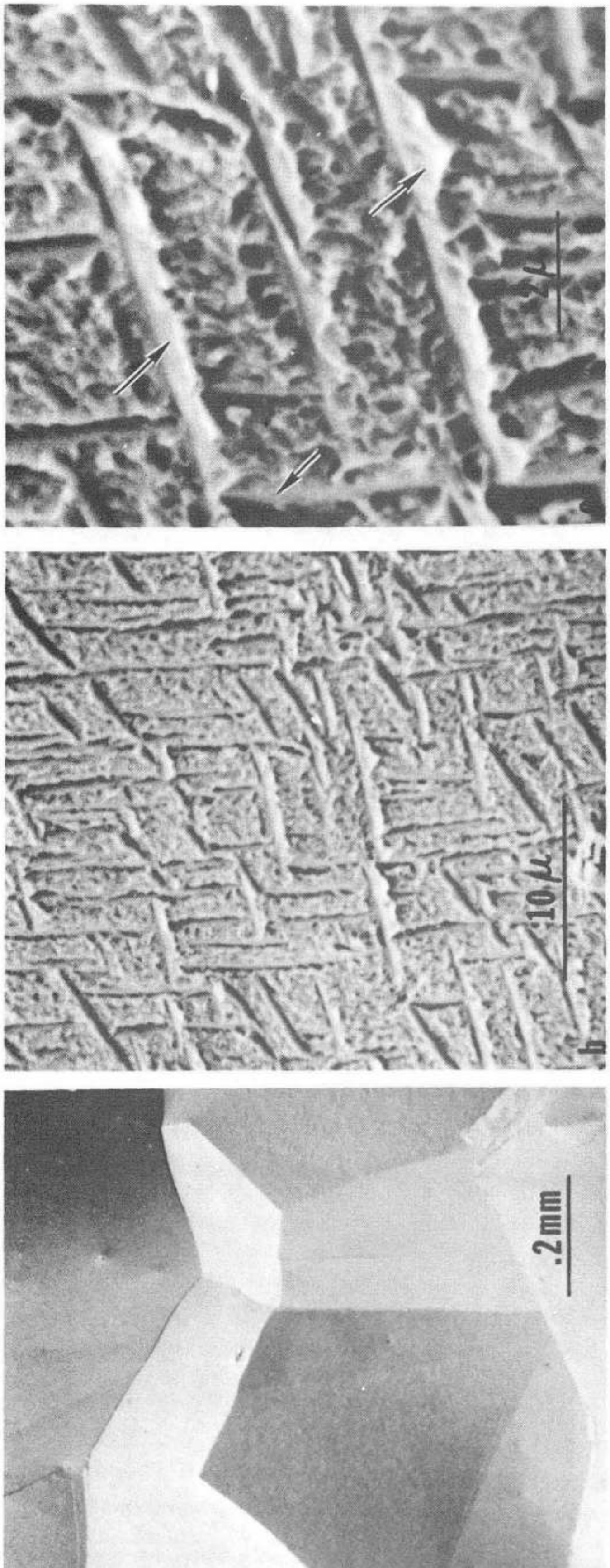

XBB 755-3898

Fig. 7

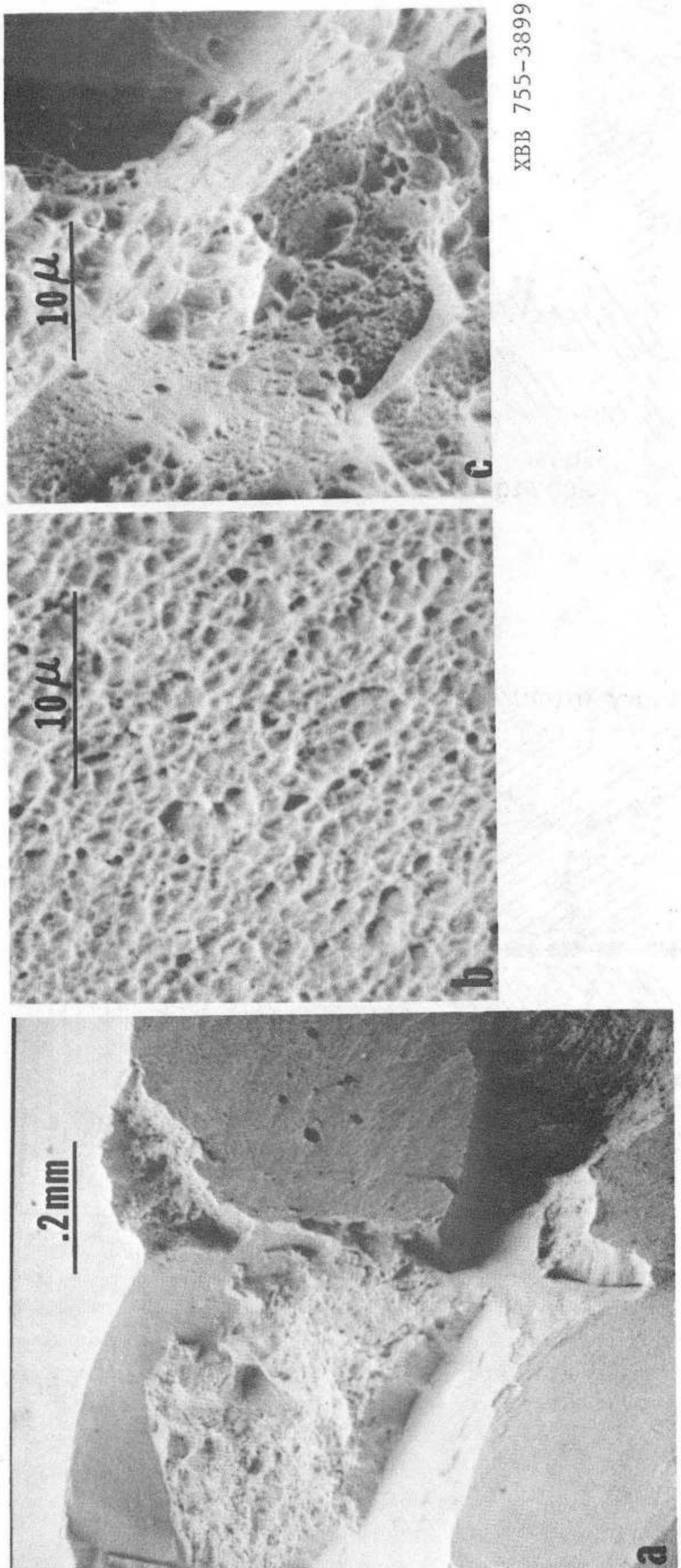

XBB 755-3899

Fig. 8

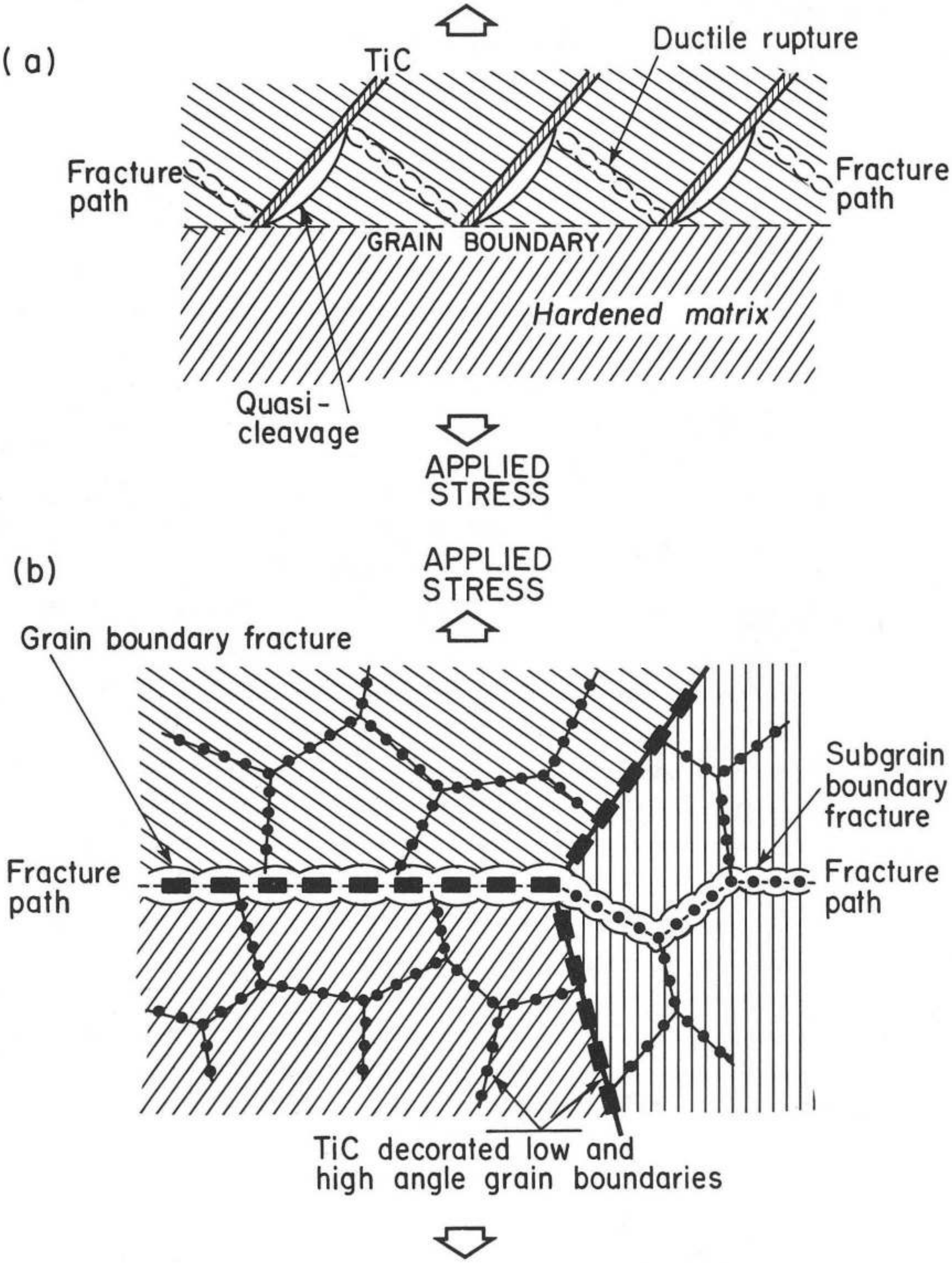

XBL 755-3048

Fig. 9

TECHNICAL INFORMATION DIVISION
LAWRENCE BERKELEY LABORATORY
UNIVERSITY OF CALIFORNIA
BERKELEY, CALIFORNIA 94720